Orbital Angular Momentum entanglement by Spontaneous Four Wave Mixing realized in a vapor by vortex beams of same handedness

Myrann Baker-Rasooli, Laurence Pruvost

Orbital Angular Momentum entanglement by Spontaneous Four Wave Mixing realized in a vapor by vortex beams of same handedness

Myrann Baker Rasooli, Laurence Pruvost*
Laboratoire de Chimie Physique-Matière et Rayonnement (LCPMR), CNRS, Sorbonne-Université, 75005 Paris France
(Dated: July 28, 2023)

Spontaneous Four Wave Mixing (SFWM) carried out in a vapor by two optical vortex beams is analyzed in the case of same handedness input orbital angular momenta. We show that the generated pair of waves carries orbital angular momenta whose entanglement strongly depends on the chosen four-levels atomic scheme, asymmetric or not. The illustration is done with two schemes of rubidium. In addition based on a theory-experiment comparison we show that the output is a partially coherent superposition of modes preserving the entanglement.

I. INTRODUCTION

The route to quantum computing and simulation requires entanglement and control including a minimization of decoherence processes. Among the available quantum systems, the photon offers many quantum variables that can be entangled through light-matter interaction. One of them is the photonic Orbital Angular Momentum (OAM) which is associated to optical vortex beam.

The first ideas about optical vortex were introduced by Coullet et al. [1] before Allen et al. defined its OAM [2]. The first experimental realizations followed [3, 4]. Then, many applications of vortex beams appeared in many fields. A review can be found in [5].

An optical vortex carries an helical phase whose number of branches and the handedness are given by an signed integer ℓ. Upon electromagnetic propagation and the Poynting vector analysis, the OAM is equal to $\hbar\ell$ per photon. Beside the spin angular momentum, namely the polarization, the OAM takes many values. It is the reason why, quite early, OAM was pointed out as a pertinent variable for coding, multiplexing information and for multi-space entanglement. In 2001, Mair et al. realized the first OAM-entanglement by Spontaneous Parametric Down-Conversion (SPDC) in a non-linear crystal [6].

In atomic vapors the atom-vortex interaction was first demonstrated [7] using degenerated four-wave mixing showing the OAM transfer from input to the idler beam. This experiment has opened a new field to exploit the atomic coherence and OAMs [8] followed by application to quantum memories [9, 10].

SPDC and SFWM are well-adapted for entanglement, because they produce pairs of photons correlated by physical constraints. SFWM occurs when two lasers resonantly excite atoms to a state which decays with the emission of two photons and via a short lifetime intermediate level. The excitation and decay selection rules determine how the photons are entangled. Often they are polarization-entangled. If the excitation is realized by vortex beams, they are also OAM-entangled.

In this paper we examine OAM-entanglement as SFWM is realized by two input vortex beams of same handedness applied to a four-levels system. We compare asymmetric and symmetric schemes (Fig. 1).

The analysis allows us to link the model to experimental data previously obtained on Rb atoms for the asymmetric scheme [11–14]. The model also predicts OAM-entanglement signatures for a symmetric scheme.

The model relies on fields decomposition onto Laguerre-Gaussian (LG) modes. It provides the OAM selection rules for SFWM realized with input LG modes. It gives an analytic formula for the mode decomposition of the generated beams. It explains the experimental observations and the observed partially-coherent interference patterns. In addition it allows us to predict about SFWM with vortex beams operated on a symmetric Rb four-levels scheme, where SFWM leads to OAM-entanglement signatures different from the asymmetric case.

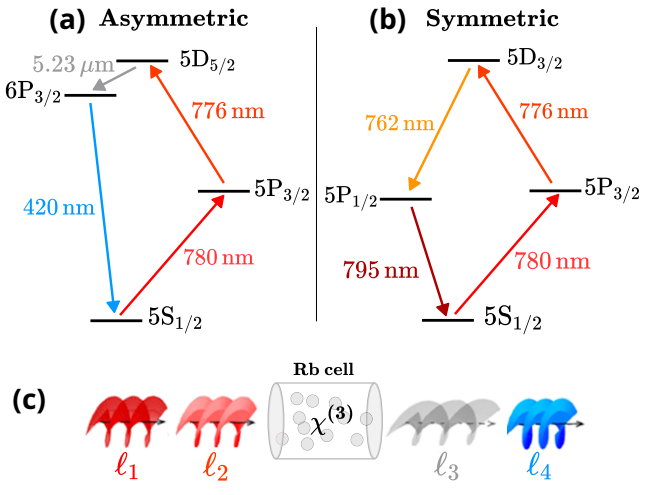

FIG. 1. Rubidium four-levels schemes and SFWM. (a) asymmetric scheme decaying via $6P_{3/2}$ level; (b) the symmetric one decaying via $6P_{3/2}$ level; (c) experiment scheme of SFWM operated with co-propagating vortex beams.

* laurence.pruvost@sorbonne-universite.fr

II. FOUR-LEVELS ATOM AND SPONTANEOUS FOUR WAVE MIXING WITH VORTEX BEAMS

A. The considered problem

We consider four-levels atomic schemes as shown in Fig.1. the atoms are excited by two lasers at wavelengths λ_1 and λ_2 and decay with two emitted waves at λ_3 and λ_4, so realizing SFWM.

For Rb atom, as treated in this paper, lasers at $\lambda_1 = 780\ nm$ and $\lambda_2 = 776\ nm$ realize the $5S \rightarrow 5D$ two-photon transition. SFWM depends on the chosen $5D$ fine level. With $5D_{5/2}$ level it produces two waves at $\lambda_3 = 5230\ nm$ and $\lambda_4 = 420\ nm$ (Fig.1(a)). Because these wavelengths are very different this case is called '*asymmetric*'. Experiments reported in [11–14] have been done with this scheme. With $5D_{3/2}$ level, SFWM produces output waves at $\lambda_3 = 762\ nm$ and $\lambda_4 = 795\ nm$ (Fig.1(b)). These wavelengths values being similar, this scheme is called '*symmetric*'.

For an atomic vapor excited by two co-propagating vortex beams carrying respectively ℓ_1 and ℓ_2 OAMs, SFWM produces two vortex beams with respectively ℓ_3 and ℓ_4 OAMs. If input beams are colinear and copropagating as shown in Fig.1(c), due to energy and linear moment conservation, the generated vortex are necessary co-propagating. Experiments of [11–14] have been realized with single-ring LG modes of same polarization as input, so the outputs are waves of same polarization.

Each generated wave results of the non-linear interaction of the 3 others. The field of the third wave E_3 is proportional to $E_1 E_2 E_4^*$. The proportional factor involves the third order susceptibility $\chi^{(3)}$ which depends of the vapor density. Respectively, E_4 is proportional to the product $E_1 E_2 E_3^*$.

B. Laguerre-Gaussian modes

All involved vortex beams of our problem are LG modes or combination of LG modes. Let us remind their expressions and main properties. A LG mode at wavelength λ is defined by its OAM ℓ and its radial number p. We denote it by a compact notation $\binom{\ell}{p}$. In cylindrical coordinates (r, θ, z), a LG mode of waist w propagating along z axis, has a Gouy number $\alpha = |\ell| + 2p + 1$ and a Rayleigh range $z_R = \pi w^2/\lambda$. Its field is expressed by

$$\binom{\ell}{p} = A_{\ell,p}\ e^{i\ell\theta}\ e^{i\alpha Atan(\frac{z}{z_R})}\ e^{i2\pi z/\lambda} \tag{1}$$

where $A_{\ell,p}$ is the amplitude.

We do not give the general expression of $A_{\ell,p}$ that can be found in [15] because only $\ell \geq 0$, $p = 0$ modes are involved in our study. The amplitude of a single-ring LG mode ($p = 0$) is

$$A_\ell = A_{\ell,0} = \sqrt{\frac{2}{\pi w^2 \ell!}}\ \left(\frac{2r^2}{w^2}\right)^{\ell/2}\ e^{-\frac{r^2}{w^2}} \tag{2}$$

It is normalized as $2\pi \int_0^\infty |A_\ell|^2 r dr = 1$ by using [16].

Such a LG mode has one ring of light whose radius R increases with ℓ as $R = w\sqrt{\ell/2}$ and whose width Δ is given by $\Delta = R^+ - R^-$ where $(R^\pm)^2 = w^2(\ell \pm \sqrt{\ell})$ are the inflection points of A_ℓ.

C. Qualitative aspects

An optimal SFWM process is obtained if, at first, the input beams overlap $J^{in} = \iint A_{\ell_1} A_{\ell_2}\ r dr d\theta$ is maximum. Using Eq.2 one gets

$$J^{in} = \frac{((\ell_1 + \ell_2)/2)!}{\sqrt{\ell_1!\ \ell_2!}} \tag{3}$$

which is maximum for $\ell_1 = \ell_2$. J^{in} allows also to define the working diagram of Fig.2(a). The yellow region indicates the favorite OAM couples (ℓ_1, ℓ_2) to be used.

The working diagram can be understood by qualitative geometric considerations. Indeed we can impose an overlap condition for the input LG modes by comparing their radii and widths as $R_2 + \Delta_2/2 > R_1 - \Delta_1/2$ and $R_2 - \Delta_2/2 < R_1 + \Delta_1/2$. This gives the following conditions $\ell_2 + \sqrt{\ell_2} > \ell_1 - \sqrt{\ell_1}$ and $\ell_2 - \sqrt{\ell_2} < \ell_1 + \sqrt{\ell_1}$ which delimite regions as shown by black lines in Fig.2(a). The lines correspond to $J^{in} \sim 0.6$.

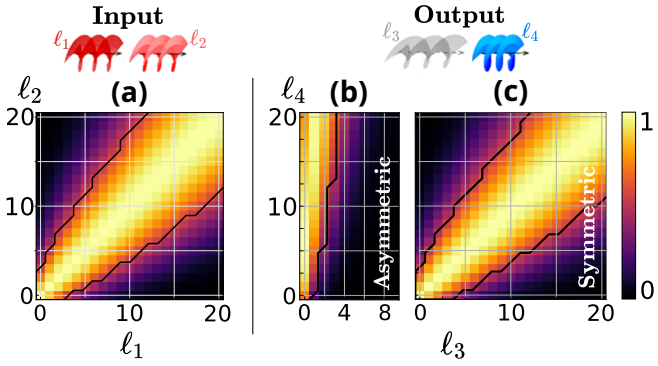

FIG. 2. Vortex beams overlap at the input and the output. (a) overlap at the input giving the working diagram; (b) overlap at the output for the asymmetric scheme; (c) overlap at the output for the symmetric scheme. The dark lines result from qualitative considerations as explained in section II.C.

Similarly, the output LG overlap can be evaluated. Assuming that output vortex beams are single-ring LG modes (demonstrated in a next section), J^{out} is defined by $J^{out} = \iint A_{\ell_3} A_{\ell_4} r dr d\theta$ and its value is

$$J^{out} = \frac{(\ell_3 + \ell_4)/2)!}{\sqrt{\ell_3!\ \ell_4!}}\ \frac{w_{out}^{\ell_3+\ell_4+2}}{w_3^{\ell_3+1}\ w_4^{\ell_4+1}} \tag{4}$$

with $\frac{2}{w_{out}^2} = \frac{1}{w_3^2} + \frac{1}{w_4^2}$.

Applying Boyd-Kleinman criterion [17], known to optimize non-linear wave mixing, which states that all involved light beams have the same Rayleigh range, we

rewrite Eq.4. Boyd-Kleinman criterion implies $w_3^2/\lambda_3 = w_4^2/\lambda_4 = w^2/\lambda$; we have put $\lambda = \lambda_1 = \lambda_2$ because the input wavelengths differ by only 0.4%. In addition because $1/\lambda_3 + 1/\lambda_4 = 2/\lambda$, it comes $w_{out} = w$ and then

$$J^{out} = \frac{((\ell_3+\ell_4)/2)!}{\sqrt{\ell_3!\ \ell_4!}} \sqrt{\frac{\lambda^{\ell_3+\ell_4+2}}{\lambda_3^{\ell_3+1}\ \lambda_4^{\ell_4+1}}} \tag{5}$$

Eq.5 shows that the output overlap J^{out} strongly depends on the output wavelengths.

For the asymmetric scheme, as $\lambda_3 \gg \lambda_4$, J^{out} is maximum at small values of ℓ_3 as shown by the yellow region of Fig.2(b). So $\ell_3 = 0$ is the most expected value in the generated pair up to $\ell_4 \sim 10$. For $\ell_4 \geq 12$ pairs with $\ell_3 = 1$ appear. The frontier is related to the wavelengths ratio $\lambda_3/\lambda_4 \sim 12$.

For the symmetric scheme, because $\lambda_3/\lambda_4 \sim 1$, the most expected output pairs satisfy $\ell_3 \sim \ell_4$ as shown by the yellow region of Fig.2(c).

Fig.2(b) and (c) illustrate how OAM-sharing in the output pair strongly depends on the four-levels scheme. We will check at this expectation by computing the output modes probability amplitudes.

III. MODEL FOR SPONTANEOUS FOUR WAVE MIXING WITH VORTEX BEAMS

A. Model and assumptions

Our approach consists in decomposing the generated waves E_3, E_4, onto a LG modes basis, the coefficients of the decomposition providing the mode probability amplitudes. Then, by propagating each mode, the intensity of the generated waves is determined at any z position. The approach differs from [18] where the model is based on the Green's function.

In the LG-decomposition model, the output pair is expressed as $\sum_{\ell_3,p_3\ell_4,p_4} c(\ell_3,p_3,\ell_4,p_4)\binom{\ell_3}{p_3}\binom{\ell_4}{p_4}$ where $c(\ell_3,p_3,\ell_4,p_4)$ is the probability amplitude of the $\binom{\ell_3}{p_3}\binom{\ell_4}{p_4}$ pair. If the mode superposition is coherent the output fields are

$$E_3 = \sum_{\ell_3,p_3,\ell_4,p_4} c(\ell_3,p_3,\ell_4,p_4)\binom{\ell_3}{p_3} \tag{6}$$

$$E_4 = \sum_{\ell_3,p_3,\ell_4,p_4} c(\ell_3,p_3,\ell_4,p_4)\binom{\ell_4}{p_4} \tag{7}$$

Fortunately, selection rules associated to SFWM process will reduce the number of involved modes and so the number of $c(\ell_3,p_3,\ell_4,p_4)$ to be determined (see section III.B). Moreover, the mathematical form of the LG modes will provide an analytical expression (III.C).

In addition, we impose assumptions related to experiments. We assume the atoms to be excited by single-ring LG beams ($p = 0$) of same waists w and carrying OAMs of the same handedness, $\ell_1 \geq 0$, $\ell_2 \geq 0$. We also assume that the medium length is short compared to the Rayleigh range z_R, so we neglect any beam divergence. In respect with the experiments, all the waves involved in SFWM have the same polarization, so the non-linear optics model is scalar.

The last assumption is Boyd-Kleinman criterion as discussed in section II.C.

B. Selection rules and allowed output pairs

SFWM is ruled by phase-matching of the involved waves from the relationship $E_3 \propto E_1 E_2 E_4^*$.

The azimutal phase-matching implies OAM conservation $\ell_3 + \ell_4 = \ell_1 + \ell_2$.

For modes with same Rayleigh range (Boyd-Kleinman criterion), the Gouy phase-matching implies the conservation of Gouy number as $\alpha_3 + \alpha_4 = \alpha_1 + \alpha_2$.

These two conditions will determine the allowed pairs of LG modes at the output. For single-ring LG modes with positive OAMs as input it gives

$$\ell_3 + \ell_4 = L \tag{8}$$

$$|\ell_3| + 2p_3 + |\ell_4| + 2p_4 = L \tag{9}$$

where $L = \ell_1 + \ell_1 \geq 0$ defines the total input OAM.

Let us analyze the solutions of Eq.8,9. If ℓ_3 and ℓ_4 are negative, it is not possible to satisfy Eq.8. If one of them is negative (e.g. ℓ_4) Eq.9 gives $\ell_4 - p_3 - p_4 = 0$ implying $p_3 = p_4 = \ell_4 = 0$ because $p_i \geq 0$. So, the only solutions are $\ell_3 \geq 0$, $\ell_4 \geq 0$ and $p_3 = p_4 = 0$. The ouputs waves are thus composed by single-ring LG modes with ℓ_3 ranging $[0, L]$ and $\ell_4 = L - \ell_3$.

The output is composed by L+1 pairs, so the fields are

$$E_3 = \sum_{\ell_3=0}^{L} c(\ell_3, L-\ell_3)\binom{\ell_3}{0} \tag{10}$$

$$E_4 = \sum_{\ell_4=0}^{L} c(L-\ell_4, \ell_4)\binom{\ell_4}{0}. \tag{11}$$

C. Probability amplitudes of output LG modes

The overlap of the four involved LG modes

$$J(\ell_3,\ell_4) = \iint A_{\ell_1} A_{\ell_2} A_{\ell_3} A_{\ell_4} r dr d\theta \tag{12}$$

is the key-quantity to get the probability amplitude $c(\ell_3,\ell_4)$ of the modes in the output, $c^2(\ell_3,\ell_4)$ being the probability to find the pair $\binom{\ell_3}{0}\binom{\ell_4}{0}$. Using the normalization factor J defined by $J^2 = \sum_{\ell_3=0}^{L} J^2(\ell_3, L-\ell_3)$ we have $c(\ell_3,\ell_4) = J(\ell_3,\ell_4)/J$.

Before computing Eq.12 we qualitatively determine the $J(\ell_3,\ell_4)$ maximum. The product of $A_{\ell_1}A_{\ell_2}$ is maximum at $r = w\sqrt{L/4}$. To get a good overlap the generated light has to be localized in this region giving an

order of magnitude for the output mode radii R_3 and R_4 and of the associated OAMs. The comparison provides $w_3\sqrt{\ell_3/2} \sim w_4\sqrt{\ell_4/2} \sim w\sqrt{L/4}$. With Boyd-Kleinman criterion we get $\ell_3 \sim \frac{\lambda}{2\lambda_3}L$ and $\ell_4 \sim \frac{\lambda}{2\lambda_4}L$.

For the asymmetric scheme it leads to $\ell_3 \sim 0.07L$ and $\ell_4 \sim 0.93L$. So, for L less than ~ 12 the output would mainly contain the $(0, L)$ pair, the OAM being preferentially transferred to wave 4 (at 420 nm). For larger values of L the pair $(1, L–1)$ would appear, then the $(2, L–2)$ one and so on. A completely different OAM-sharing would occur in the symmetric scheme because $\ell_3 \sim 0.5L$ and $\ell_4 \sim 0.6L$.

Using Eq.2 and note [19] we establish

$$J(\ell_3, \ell_4) = \frac{2}{\pi}\frac{L!}{\sqrt{\ell_1!\ell_2!}}\frac{w_t^{2L+2}}{w^{L+2}}\frac{1}{\sqrt{\ell_3!\ell_4!}}\frac{1}{w_3^{\ell_3+1}w_4^{\ell_4+1}} \quad (13)$$

with $\frac{2}{w_t^2} = \frac{2}{w^2} + \frac{1}{w_3^2} + \frac{1}{w_4^2}$.

For a given input set, the ℓ_3, ℓ_4 dependence in Eq.13 comes from the two last terms. We can thus ignore the pre-factor which will disappear in the normalization and so avoid to compute time-consuming factorials.

Furthermore, because $\ell_4 = L-\ell_3$, the amplitude $c(\ell_3, L-\ell_3)$ can be expressed as

$$c(\ell_3, L-\ell_3) = \frac{1}{c}\sqrt{\frac{L!}{\ell_3!(L-\ell_3)!}}\frac{1}{w_3^{\ell_3}w_4^{L-\ell_3}}$$

with $c^2 = \sum_{\ell_3=0}^{L}\frac{L!}{\ell_3!(L-\ell_3)!}(\frac{1}{w_3^2})^{\ell_3}(\frac{1}{w_4^2})^{L-\ell_3}$. We recognize the binomial formula $c^2 = (\frac{1}{w_3^2} + \frac{1}{w_4^2})^L \equiv (\frac{2}{w_{out}^2})^L$. Then

$$c(\ell_3, L-\ell_3) = \sqrt{\frac{L!}{\ell_3!(L-\ell_3)!}}\frac{(w_{out}/\sqrt{2})^L}{w_3^{\ell_3}w_4^{L-\ell_3}} \quad (14)$$

Eq.14 provides an analytical expression of the amplitude probability, which is valid for any four-levels schemes of atoms even different of rubidium.

It is convenient to express Eq.14 versus wavelengths rather than waists. Applying Boyd-Kleinman criterion and energy conservation $(2/\lambda = 1/\lambda_3 + 1/\lambda_4)$ it becomes

$$c(\ell_3, L-\ell_3) = \sqrt{\frac{L!}{\ell_3!(L-\ell_3)!}\frac{\lambda^L}{2^L\lambda_3^{\ell_3}\lambda_4^{L-\ell_3}}} \quad (15)$$

Eq.15 shows a crucial dependence of the output versus the ratio $\frac{\lambda_4}{\lambda_3}$. This is illustrated in the following section.

IV. APPLICATION TO ASYMMETRIC AND SYMMETRIC SCHEMES OF RUBIDIUM

In this section the LG-decomposition method is applied to rubidium schemes of Fig.1, to compare with available experimental data (asymmetric) or to predict patterns in the case of symmetric scheme.

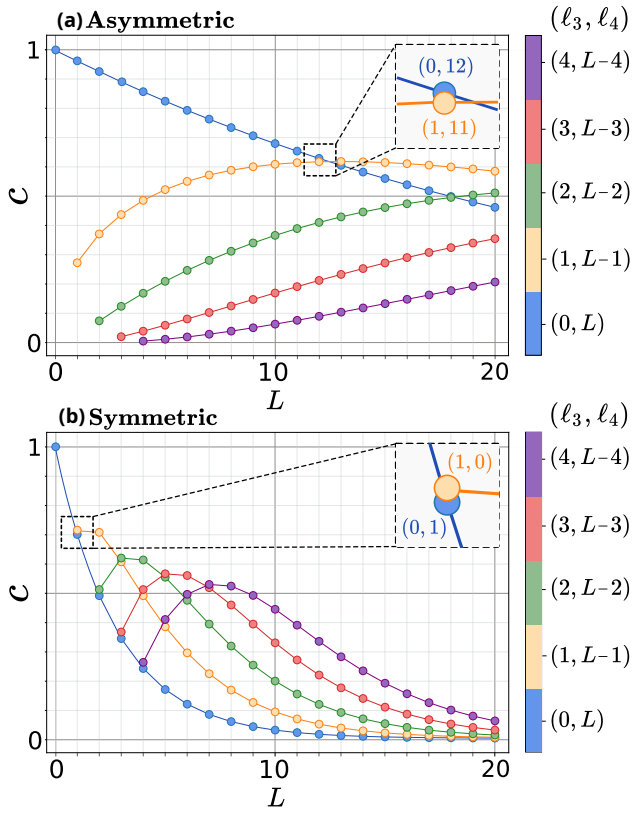

FIG. 3. Mode analysis of the output : probability amplitudes of modes versus the total input OAM. (a) for the asymmetric scheme; (b) for the symmetric scheme. Blue, orange, green, red and purple curves correspond to pair families (ℓ_3, ℓ_4) for $\ell_3 = 0$ to 4. The insets show details where the families $(0, L)$ and $(1, L-1)$ are crossing.

A. Probability amplitudes

Fig.3 presents the probability amplitudes $c(\ell_3, L-\ell_3)$ versus the total input OAM L for $\ell_3 = 0$ to 4. Each plot color represents a pair family, blue for the $(0, L)$ one, orange for $(1, L-1)$ one and so on. The insets show the first L for which probability amplitudes are equal, namely $L = 12$ for the asymmetric scheme and $L = 1$ for the symmetric one.

For the asymmetric scheme, Fig.3(a) shows that the $(0, L)$ pair dominates in the output if $L < 12$. In this case the input OAM L is mostly transferred to wave 4 (i.e. the blue light). For $L > 12$ the pair $(1, L-1)$ becomes the most probable in the output. Around $L = 12$ the output contains mainly the two pairs, $(0, 12)$ and $(1, 11)$, the other being of weaker probability. In this L region, ℓ_3-ℓ_4 being entangled, the question of family entanglement is open.

The symmetric scheme (Fig.3(b)) has a completely different behavior. Plots probability amplitudes exhibit maximums in succession, each maximum corresponding to the pair $(L/2, L/2)$, which indicates an equitable OAM-sharing in the output waves. Fig.3(b) shows more

crossing of the families, also at low values of L, indicating a multimode character which appears at low L values. For example, at $L = 1$ the pairs $(0, 1)$ and $(1, 0)$ are 50/50 mixed, which is different in a asymmetric case.

B. Experimental SFWM with vortex beams

Some elements are given here to describe the detected signals in experiments and their signatures.

The principle of experiments reported in [11–14] consists to apply to a rubidium vapor at about hundred degrees, two lasers beams previously phase-shaped into a LG mode, in general using a spatial light modulator. The beams are superimposed colinear co-propagating and with the same circular polarization in order to optimize the two-photon transition.

The waves generated by SFWM are extracted by wavelength separation (filter or prism) and analyzed in intensity and in phase. In the mentioned experiments the generated blue beam at 420 nm has been detected. The intensity after propagation (at $z = \infty$) has been recorded on a CCD camera. The phase of the beam is analyzed by optics interference.

Fig.4 gives a scheme of the detection used by A. Chopinaud in his PhD work [15] with intensity detection on CDD1 and phase detection on CCD2 after passing through a modified Mach-Zehnder interferometer. The "Dove-Mach-Zehnder" (DMZ) interferometer includes a Dove prism which returns the field. If the DMZ interferometer is addressed by a pure LG beam carrying the OAM ℓ then it produces an azimuthally-modulated pattern (flower pattern) having a 2ℓ spatial frequency. Fig.4 shows the intensity and interference pattern of the blue SFWM-generated beam obtained for $L = 2$.

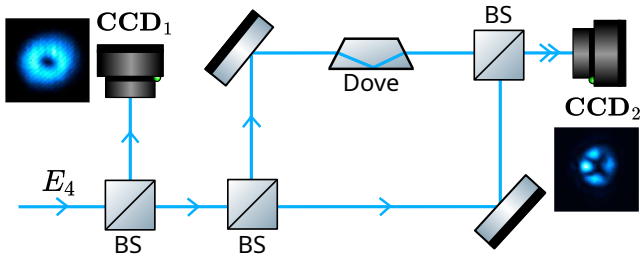

FIG. 4. Detection of the intensity of wave 4 (CCD_1) and of its phase by a Dove-Mach-Zehnder interferometer (CCD_2). Intensity and interference patterns recorded for $L = 2$.

C. OAM-entanglement signatures

The LG-decomposition model is used to compute intensity and DMZ interference patterns in order to compare with experimental ones. We examine two situations, one where the generated fields are fully coherent, the other with partial coherence.

For both cases the field is considered at $z = \infty$. The modification to put concerns the Gouy phase which change for each LG mode due to the propagation. For the ℓ_4 component the Gouy phase is then $\pi(\ell_4 + 1)/2$.

For fully coherent fields the beam intensity is

$$I_\infty = \left| \sum_{\ell_4=0}^{L} c(L-\ell_4, \ell_4) \binom{\ell_4}{0} \right|^2 \tag{16}$$

and the DMZ pattern is

$$I_\infty^{\mathrm{DMZ}} = \left| \sum_{\ell_4=0}^{L} c(L-\ell_4, \ell_4) \left[\binom{\ell_4}{0} + \binom{-\ell_4}{0} \right] \right|^2 \tag{17}$$

Eqs.16-17 computed for $L = 2, 10, 20$ with experimental parameters given in [15] provide plots of Fig.5(a). They have been scaled to be compared to Fig.5(c) pictures. The wave 4 intensities exhibit shapes as crescent moon, which is not the case in Fig.5(c). Even if we introduce a relative azimuthal phase between the LG modes component (also random) the intensity is never perfectly annular like in Fig.5(c). The DMZ interference patterns show large modulations on the bright fringes. For $L = 10$ and 20 the bright fringes intensity goes down the mean intensity value. Also for $L = 20$ a part of the pattern is nearly dark. Such modulation is not observed on the experimental data. That suggests a partial coherence.

With the assumption of partially coherent mode composition the intensity is

$$\langle I_\infty \rangle = \sum_{\ell_4=0}^{L} c^2(L-\ell_4, \ell_4) \left| \binom{\ell_4}{0} \right|^2 \tag{18}$$

and its DMZ pattern is

$$\langle I_\infty^{\mathrm{DMZ}} \rangle = \sum_{\ell_4=0}^{L} c^2(L-\ell_4, \ell_4) \left| \binom{\ell_4}{0} + \binom{-\ell_4}{0} \right|^2 \tag{19}$$

Fig.5(b) shows the patterns computed by Eqs.18-19 with the same experimental parameter as before. As expected the wave 4 intensities are ring-shaped. The DMZ interference patterns keep azimuthal modulations, but the bright fringes never go down the mean intensity value. It corresponds to observed data of Fig.5(c).

In addition we observe blurred regions and an alternating contrast along the light ring. Such an observation is viewed in the experimental patterns, making it difficult to count the fringe number. The alternating contrast is well-reproduced if the relative phase between the modes equals zero. This indicates that the generated modes keep the same starting point for their azimuthal phase. It is imposed by the input vortex beams and the third order non-linear effect.

Even if the output is a partially coherent superposition of modes, signatures of the mode composition and thus of the output pair families still persist in the DMZ

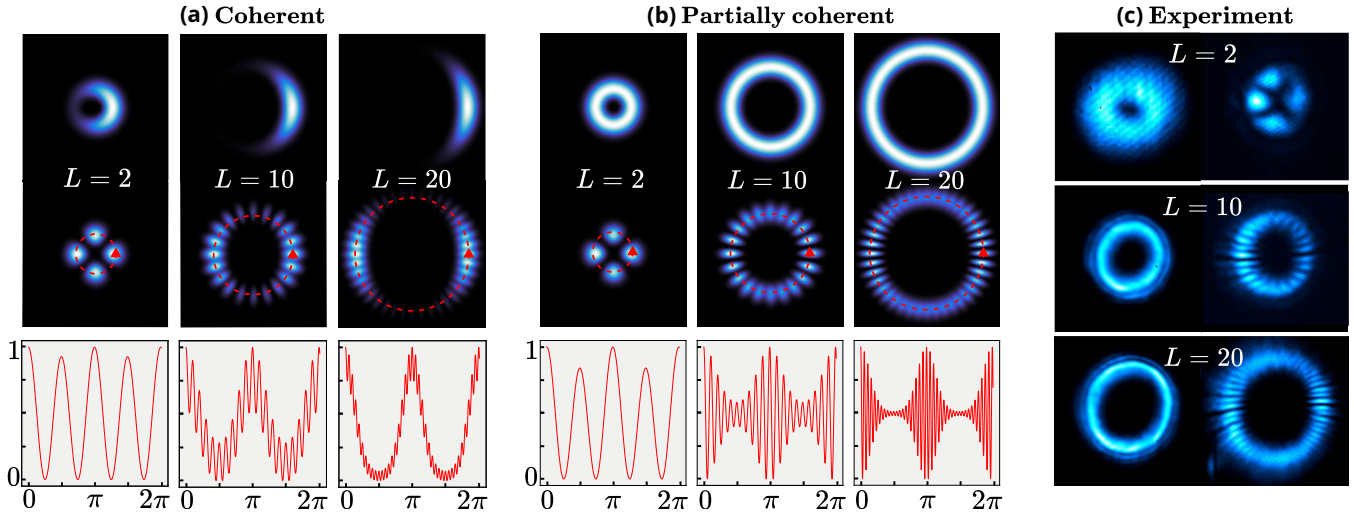

FIG. 5. Intensities and DMZ interference patterns of wave 4, for the asymmetric scheme, for $L = 2, 10$ and 20. (a) fully-coherent emission; (b) partially-coherent case as explained in IV.C. (c) experimental data from [15], intensities on the left and DMZ patterns on the right. Red curves are azimuthal intensity profiles along the above indicated red dotted lines.

interference pattern. They are the fringes, their number and the contrast. In principle the decomposition of the blue beam over LG modes could be extracted either by a fit procedure or by a decomposition of the DMZ azimuthal profile as a Fourier series. It would be tested in a forthcoming work using systematic data and a wide range of input OAM values. The key to get the information relies on the generation in phase in SFWM, of the two generated waves.

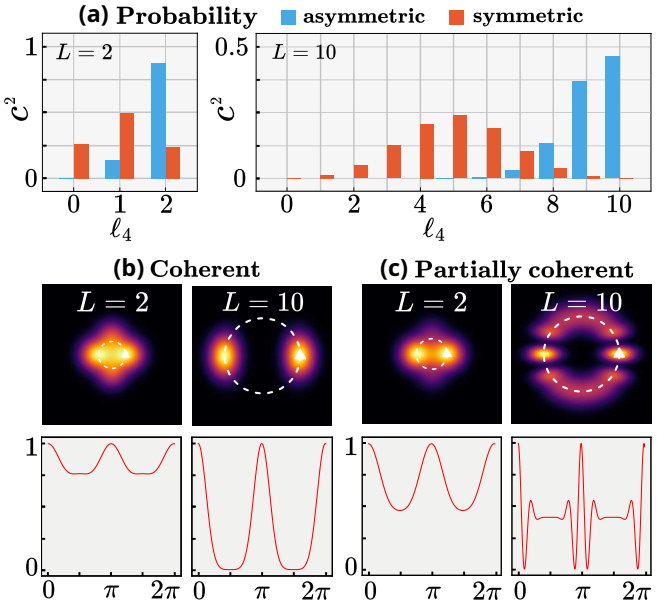

FIG. 6. DMZ interference patterns for the symmetric scheme, for $L = 2$ and 10. (a) Output mode probabilities, symmetric (orange) compared to asymmetric (blue). (b) Patterns for a fully-coherent emission. (c) Patterns for a partially-coherent emission. Red curves are azimuthal intensity profiles along the above indicated white dotted lines.

To end this study, we aim to predict at OAM-entanglement signatures for the symmetric scheme. For that, the DMZ interference patterns have been computed using this LG-decomposition model. The results for $L = 2$ and 10 are shown in Fig.6(b,c).

The DMZ interference patterns have completely different forms from those obtained for asymmetric case. They exhibit fringes with a stronger blurring and the number of fringes is far from $2L$. It is due to the output decomposition (orange bars in Fig.6(a)) which is broad and has a maximum at $\ell_4 \sim L/2$. The probabilities for the asymmetric scheme is rather maximum at $\ell_4 \sim L$ (blue bars in Fig.6(a)).

The prediction could be validated with experiments. The deduced decomposition of the blue beam over LG modes using a Fourier series transform of the DMZ interference patterns could be tested.

V. CONCLUSION

The LG-decomposition method to determine generated pairs in the SFWM process has been developed providing an analytical formula (Eq. 14) of mode probability amplitudes. The formula is valid for any four-level scheme of atomic systems.

The method has been applied to analyze experimental data previously obtained for the asymmetric scheme of rubidium. It shows that SFWM produces OAM-entangled pairs which are partially-coherent but which have the same azimuthal phase starting point. This confirms the strong constraint in phase imposed by the third order non-linear process and that its 'spontaneous' character is not intuitive.

In addition, the LG-decomposition method gives prediction about the symmetric four-levels scheme, with sig-

natures in the DMZ pattern expected to be different. This opens to experiments where multi-dimensional entanglement would appear.

Acknowledgments: The authors thank Région Ile de france, DIM SIRTEQ (Science et Ingénierie en Région Ile-de-France pour les Technologies Quantiques) and DIM QuanTiP (Quantum Technologies in Paris Region) for financial supports especially for a PhD grant and for scientific equipments.

L.P. thanks Université Paris-Saclay (previous affectation) for supports allocated by the Labex PALM and by IQUPS, Laboratoire A Cotton (LAC, UMR 9025) for past technical supports, and Institut des sciences moléculaires d'Orsay (ISMO, UMR 8214) for the great hospitality during the laboratory renovation.

[1] P. Coullet, L. Gil and F. Rocca, Optical vortices, Opt. Comm. **73**, 403 (1989).

[2] L. Allen, M. W. Beijersbergen, R. J. C. Spreeuw, and J. P. Woerdman, Orbital angular momentum of light and the transformation of Laguerre-Gaussian laser modes, Phys. Rev. A **45**, 8185 (1992).

[3] M. W. Beijersbergen, R. P. C. Coerwinkel, M. Kristensen, J. P. Woerdman, Helical-wavefront laser beams produced with a spiral phaseplate, Opt. Comm. **112**, 321 (1994).

[4] M. Padgett, J. Arlt, N. Simpson, L. Allen, An experiment to observe the intensity and phase structure of Laguerre-Gaussian laser modes, Am. J. of Phys. **64**, 77 (1996).

[5] Y. Shen, X. Wang, Z. Xie et al., Optical vortices 30 years on: OAM manipulation from topological charge to multiple singularities, Light Sci Appl. **8**, 90 (2019).

[6] A. Mair , A. Vaziri, G. Weihs, A. Zeilinger, Entanglement of the orbital angular momentum states of photons, Nature **412**, 313 (2001).

[7] J. W. R. Tabosa, D. V. Petrov, Optical Pumping of Orbital Angular Momentum of Light in Cold Cesium Atoms, Phys. Rev. Lett. **83**, 4967 (1999).

[8] S. Barreiro, J. W. R. Tabosa, Generation of Light Carrying Orbital Angular Momentum via Induced Coherence Grating in Cold Atoms, Phys. Rev. Lett. **90**, 133001 (2003).

[9] A. J. de Almeida, S. Barreiro, W. S. Martins, R. A. de Oliveira, D. Felinto, L. Pruvost, J. W. R. Tabosa, Storage of orbital angular momenta of light via coherent population oscillation. Opt Lett. **40**, 2545 (2015).

[10] . A. Nicolas, L. Veissier, L. Giner et al., A quantum memory for orbital angular momentum photonic qubits, Nature Phot. **8**, 234 (2014).

[11] A. Chopinaud, M. Jacquey, B. Viaris de Lesegno, L. Pruvost, High helicity vortex conversion in a rubidium vapor, Phys. Rev. A **97**, 063806 (2018).

[12] G. Walker, A. S. Arnold, and S. Franke-Arnold, Trans-Spectral Orbital Angular Momentum Transfer via Four-Wave Mixing in Rb Vapor, Phys. Rev. Lett. **108**, 243601 (2012).

[13] A. M. Akulshin, I. Novikova, E. E. Mikhailov, S. A. Suslov, and R. J. McLean, Arithmetic with optical topological charges in stepwise-excited Rb vapor, Opt. Lett. **41**, 1146 (2016).

[14] N. Liu, X. Wang, J. Yuan, L. Xiao, S. Jia and L. Wang, Manipulation of the orbital angular momentum via four-wave mixing in Rb vapor, Laser Phys. Lett. **20**, 035204 (2023).

[15] A. Chopinaud, Atomes et vortex optiques : conversion de moments orbitaux de lumière en utilisant la transition à deux photons 5S-5D du rubidium, PhD thesis, Université Paris-Saclay (2018), https://theses.hal.science/tel-01941723.

[16] The integral is computed by putting $X = \frac{2r^2}{w^2}$ and using $\int_0^\infty X^\ell\, e^{-X} dX = \ell!$ with $\ell! = \Gamma(\ell+1)$ if ℓ is not integer, Γ being the gamma function. This property will also be used in the section III.

[17] G. D. Boyd, D. A. Kleinman, Parametric Interaction of Focused Gaussian Light Beams. J. Appl. Phys. **39**, 8 (1968)

[18] R. N. Lanning, Z. Xiao, M. Zhang, I. Novikova, E. E. Mikhailov, and J. P. Dowling, Gaussian-beam-propagation theory for nonlinear optics involving an analytical treatment of orbital-angular-momentum transfer Phys. Rev. A **96**, 013830 (2017).

[19] Starting from

$$J(\ell_3,\ell_4) = \iint \sqrt{\frac{2}{\pi w^2 \ell_1!}}\sqrt{\frac{2}{\pi w^2 \ell_2!}}\left(\frac{2r^2}{w^2}\right)^{L/2} e^{-\frac{2r^2}{w^2}} \sqrt{\frac{2}{\pi w_3^2 \ell_3!}}\left(\frac{2r^2}{w_3^2}\right)^{\ell_3/2} e^{-\frac{r^2}{w_3^2}} \sqrt{\frac{2}{\pi w_4^2 \ell_4!}}\left(\frac{2r^2}{w_4^2}\right)^{\ell_4/2} e^{-\frac{r^2}{w_4^2}} r dr d\theta$$

we introduce $\frac{2}{w_t^2} = \frac{2}{w^2} + \frac{1}{w_3^2} + \frac{1}{w_4^2}$ so

$$J(\ell_3,\ell_4) = 2\pi \sqrt{\frac{2}{\pi w^2 \ell_1!}}\sqrt{\frac{2}{\pi w^2 \ell_2!}}\sqrt{\frac{2}{\pi w_3^2 \ell_3!}}\sqrt{\frac{2}{\pi w_4^2 \ell_4!}} \frac{w_t^{2L}}{w_1^{\ell_1} w_2^{\ell_2} w_3^{\ell_3} w_4^{\ell_4}} \int \left(\frac{2r^2}{w_t^2}\right)^L e^{-\frac{2r^2}{w_t^2}} r dr$$

Then, with [16] one gets Eq. 13.